Geometrical fitting of experimental XANES spectra by a full multiple-scattering procedure

M. Benfatto[a]* and S. Della Longa[b,c]

[a]*LNF–INFN–PO Box 13-00044 Frascati, Italy,*
[b]*Dip. Medicina Sperimentale, Univ. L'Aquila, via Vetoio – 67100 – L' Aquila, Italy, and* [c]*INFM – Un. Roma I, Pza A. Moro – 00185 – Roma, Italy. E-mail: benfatto@lnf.infn.it*

In this paper a new software procedure is presented, named *MXAN*, able to fit the XANES part (from the edge to about 200 eV) of experimental X-ray absorption data. The method is based on the fitting between the experimental spectrum and several theoretical calculations generated by changing the relevant geometrical parameters of the site around the absorbing atom. The X-ray photo-absorption cross section is calculated using the full multiple-scattering scheme; different choices of the exchange correlation part of the potential can be utilised. To show the potentialities of the method the analysis of the nickel *K*-edge of the nickel ion in aqueous solution is presented. The procedure is able to recover the correct information on the symmetry and atomic distances from the experimental Ni *K*-edge XANES spectrum. The recovered structure is found to be independent of the starting conditions, showing the theoretical uniqueness of the structural solution.

Keywords: X-ray absorption near-edge spectroscopy (XANES); data analysis.

1. Introduction

X-ray absorption spectroscopy (XAS) is a powerful method for obtaining both electronic and structural information on the site around the absorbing atom of different types of matter. The fit in terms of the local geometrical structure of the low-energy part of the XAS spectrum, *i.e.* from the rising edge up to a few hundreds of eV, the so called XANES (X-ray absorption near-edge structure) region, has long been an aim of users of this technique, especially in the cases of limited *k*-range experimental data where a standard EXAFS (extended X-ray absorption fine structure) analysis cannot be easily performed.

The XANES part is extremely sensitive to the structural details of the absorbing site (overall symmetry, distances and angles), so that, in principle, an almost complete recovery of the geometrical structure within 6–7 Å from the absorber can be achieved from the experimental spectrum. A further advantage lies in the limited effects of the atomic thermal disorder, *i.e.* Debye–Waller-like terms, due to the fact that any signal associated with the *n*th multiple-scattering (MS) event can be written as a sine function whose argument is given by $2kR_{tot} + F(k, \mathbf{R}_i,…,\mathbf{R}_n)$; R_{tot} is the total length of the MS path of order *n* (Benfatto *et al.*, 1986). As a consequence, the associated total Debye–Waller damping factor contains always a term like $\exp(-2k^2\sigma^2)$, coming from the 'geometrical' part R_{tot}. This is the dominant term and is almost temperature independent and equal to unity in the low-energy part of the spectrum, *i.e.* for small *k* values.

However, the quantitative analysis of the XANES spectra presents some difficulties mainly due to the theoretical approximation in the treatment of the potential (Tyson *et al.*, 1992; Binsted & Hasnain, 1996) and the need for heavy time-consuming

algorithms (Durham *et al.*, 1982) to calculate the absorbing cross section in the framework of the full multiple-scattering approach (Natoli & Benfatto, 1986). For these reasons, the 'XANES analysis' is so far considered a 'qualitative' technique, used as a help for standard EXAFS studies (Michalowicz, 1997) or more advanced investigations like the ones based on the analysis of contributions related to correlation functions of orders higher than two (Filipponi & Di Cicco, 1995). Few attempts have been made so far to study the theoretical sensitivity of XANES to structural parameters and few examples of quantitative comparison between experimental data and *ab initio* calculations can be found in the literature and almost related to known structural compounds (Della Longa *et al.*, 1995; Della Longa *et al.*, 1998).

The possibility to perform quantitative XANES analysis to obtain a structural determination of an unknown compound can be relevant in many scientific fields, like extra-dilute systems, trace-element analysis, local investigation of materials under extreme conditions and much more in biological systems where the low S/N ratio and the weak scattering power of the light elements limits the *k*-range of the available experimental data. Moreover, the structural information on protein metal sites can be obtained with atomic resolution in any state of the protein sample (crystal, solution), allowing either the comparison with already known X-ray structures at high resolution or to obtain information on proteins that have proven difficult to crystallise (Hasnain & Hodgson, 1999; Cruickshank, 1999).

In this paper we present a new software package, named *MXAN*, to obtain a reliable fit of the experimental data in terms of a defined set of structural parameters. The *MXAN* package makes use of the *CONTINUUM* code (Natoli & Benfatto, 1986) to calculate the absorbing cross section in the framework of the full MS approach, *i.e.* the scattering path operator is calculated exactly, without any series expansion. Starting from a putative geometrical configuration of the absorbing site, this package is able to reach best-fit conditions in reasonable time by the minimization of the square residual function in the parameter space. It uses the *MINUIT* routines of the CERN library (James, 1994); the calculations are performed in the energy space without involving any Fourier transform algorithm; polarized spectra can be easily analysed because the calculations are performed by the full MS approach.

In the present work, we first evaluate the precision of the *MXAN* procedure by following the theoretical behaviour of the square residual function along a theory-*vs*-theory optimization procedure; then, as a real case, we report the best-fit results related to the experimental data of the Ni *K*-edge of the Ni^{2+} ion in aqueous solution. We have chosen the XANES spectrum of the *K*-edge of the Ni^{2+} octahedral system in aqueous solution because this system is normally used as both a reference compound in the analysis of other materials and a test system of theoretical calculations due to the well defined formal valency of the ionic species and the very simple geometry around the absorber (Garcia *et al.*, 1986; Briois *et al.*, 1995; Benfatto *et al.*, 1997). The Ni^{2+} in aqueous solution is an octahedral-coordinated compound with an oxygen–metal distance of about 2.0 Å; previous EXAFS investigations found an average oxygen–metal distance of 2.02 ± 0.03 Å (Lagarde *et al.*, 1980; Enderby & Neilson, 1981).

2. The *MXAN* procedure

The method is based on the comparison between the experimental spectrum and several theoretical calculations performed by changing selected structural parameters from a starting putative structure, *i.e.* from an initial configuration of the atoms around the absorber. A

1087

simple sketch of the computational procedure is depicted in Fig. 1. The X-ray photoabsorption cross section is calculated using the general MS scheme within the muffin tin (MT) approximation (Durham *et al.*, 1982; Natoli & Benfatto, 1986; Tyson *et al.*, 1992) with the MT radii chosen according to the Norman criterion (Norman, 1976). The exchange and correlation part of the potential is determined on the basis of the local density approximation of the self-energy of the excited photoelectron using an opportune complex optical potential (Tyson *et al.*, 1992). This approach makes the analysis of the high-energy part of the spectrum a quantitative tool for structural analysis and provides a reasonably good approximation for the low-energy part, as exemplified by many applications. Actually, the *MXAN* procedure can use either the X_α energy-independent potential or the complex Hedin–Lunqvist (HL) energy-dependent potential (Hedin & Lundqvist, 1969). The calculated spectra are then convoluted with a Loretzian function of constant width to mimic the spectral broadening due to the core-hole lifetime and the experimental resolution. The user either chooses the value of the Lorentzian width or it can be finely fitted by the *MXAN* procedure. In molecular systems, the complex part of the HL potential introduces an excessive loss in the transition amplitude of the primary channel that carries out all the structural information (Benfatto *et al.*, 1997; Rehr & Albers, 2000). For this reason, it is
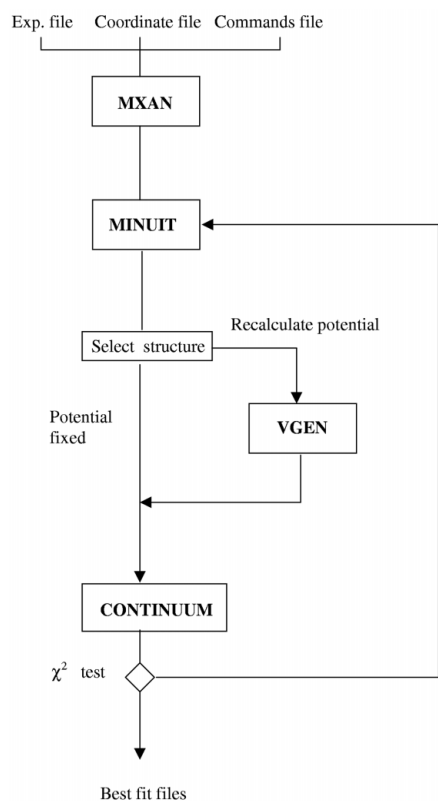
also possible to account for all the inelastic processes by a convolution of the total cross section, calculated on the basis of a real potential, with a broadening Lorentzian function having a width given by $\Gamma = \Gamma_c + \Gamma(E)$. The constant part includes the core-hole lifetime and the experimental resolution, while the energy-dependent term represents all the intrinsic and extrinsic inelastic processes. The energy-dependent part is zero below the Fermi energy, behaves like the universal form of the mean free path (Muller *et al.*, 1982) and contains a jump at an energy that in extended systems corresponds to plasmon excitations. The user must initially choose this energy and jump, and then they are adjusted during the fit by the *MXAN* procedure. This type of approach is justified on the basis of a multi-channel multiple-scattering theory (Natoli *et al.*, 1990). In the sudden limit, the net absorption is given by a sum over all the possible channels that represent each of the final states allowed in the photoabsorption process (Chou *et al.*, 1987; Natoli *et al.*, 1990). They include the fully relaxed configuration, the primary channel, which gives the main contribution to the spectrum, and all the other possible excited states of the $(N-1)$-electron system. By assuming that the channels coming from the excitation of the $N-1$ electrons are very near in energy, the total absorption is given by a convolution of the one-particle spectrum calculated with the full-relaxed potential with a spectral function representing the weight of the other excited states. Obviously, in the cases when contributions from one or more of these excited states become relevant, they must be considered explicitly in the calculation.

The potential can be calculated for each structural atomic configuration generated during the optimization pathway, but can be also, optionally, left fixed. This last option allows for the use of more sophisticated external potentials.

The *MXAN* procedure needs three input files containing, respectively, the experimental data to be fitted, the starting atomic coordinates of the cluster, and the commands and options necessary for the chosen minimization strategy. *MXAN* makes use of the set of programs developed by the Frascati theory group (Natoli & Benfatto, 1986; Tyson *et al.* 1992); in particular, *VGEN*, a generator of muffin tin potentials, and the *CONTINUUM* code for the full multiple-scattering cross-section calculation. The optimization in the space of the parameters is achieved using the *MINUIT* routines of the CERN library; a single best-fit procedure takes typically 8 h on a UNIX scalar α-VAX machine for a calculation involving six fitting parameters in a cluster of 35 atoms. The *MINUIT* routines minimize the square residual function

$$S^2 = n \frac{\sum_{i=1}^{m} w_i \left[\left(y_i^{th} - y_i^{exp} \right) \varepsilon_i^{-1} \right]^2}{\sum_{i=1}^{m} w_i}$$

where n is the number of independent parameters, m the number of data points, y_i^{th} and y_i^{exp} the theoretical and experimental values of absorption, ε_i the individual errors in the experimental data set, and w_i is a statistical weight. For $w_i = \text{constant} = 1$, the square residual function S^2 becomes the statistical χ^2 function.

The XANES analysis in real applications can be sometimes affected by systematic errors because of the approximations in the numerical molecular potential determination. In particular, the MT approximation (Foulis *et al.*, 1995; Cabaret *et al.*, 1999) for the shape of the potential, and the use of an optical potential to take into account in an average way many-body processes relevant in the low-

Figure 1
Logical sketch of the *MXAN* procedure. The main computational units are included in bold within rectangles.

energy region of the XAS spectrum. The relevance of such effects is strongly system-dependent and not known *a priori* for any system, although some general considerations can be made. Open systems and small molecules can be more affected by these errors.

The effect of the MT approximation can be clarified by writing the total cross section $\sigma_t(E)$ as a sum of two terms: the first is the total cross section calculated on the basis of the MT approximation; the second includes corrections which are proportional to both the volume of the interstitial region and the magnitude of the deviations from a constant value of the interstitial potential. In fact, $\sigma_t(E)$ is proportional to $\underline{\text{Im}}(\underline{T} + \underline{H})^{-1}$ where $\underline{T} = (T_a)^{-1} + \Delta T$ and $\underline{H} = H + \Delta H$. Here $(T_a)^{-1}$ and H are the usual MS quantities calculated in the MT approximation (Natoli *et al.*, 1986; Tyson *et al.*, 1992), while ΔT and ΔH are corrections proportional to integrals over the interstitial volume (Natoli *et al.*, 1986). The quantity $(\underline{T} + \underline{H})^{-1}$ can be written as $[(T_a)^{-1} + H + \Delta)]^{-1}$ where $\Delta = \Delta T + \Delta H$. It can be expanded in series using Δ as parameter. In this way, $\sigma_t(E)$ becomes:

$$\sigma_t(E) \propto \text{Im}\left\{ \sum_{n=0}^{\infty} (-1)^n [(T_a^{-1} + H)^{-1}\Delta]^n (T_a^{-1} + H)^{-1} \right\}$$
$$= \text{Im}\left\{ (T_a^{-1} + H)^{-1} - (T_a^{-1} + H)^{-1}\Delta(T_a^{-1} + H)^{-1} + \ldots \right\}$$
$$= \sigma_t^{MT}(E) + \text{corr.}(E)$$

From this point of view, the MT form for the shape of a molecular potential can be regarded as the zero-order approximation of a full potential calculation. The non-MT term corr.(E) depends on the system and goes to zero as the energy increases; for closed packed structures, corr.(E) is small in the whole energy range, while according to recent applications to open structures (Foulis *et al.*, 1995; Cabaret *et al.* 1999) it can be relevant within the first 20 eV from the edge.

As a general consideration, the higher the energy of the photoelectron, the lower the artificial due to the errors in the potential determination, because they are typically of the order of a few eV. To minimize the effect on the numerical results, it is possible to introduce a statistical weight w_i in the fitting procedure. In the first part of this work we have used an arctangent function defined as:

$$w_i = 0.5 + \frac{1}{\pi}\text{arctg}\left(\frac{E_i - E_c}{\Theta}\right)$$

with the parameters E_c and Θ equal to 30 eV and 10 eV, respectively. This choice implies that the energy region of the maximum of the spectrum (10 eV from the edge) weights for about the 15% relative to the high-energy part. Even if no particular physical meaning is related to the parameters E_c and Θ, this choice allows selecting the energy range with the most reasonable theoretical confidence with the experiments, without losing sensitivity to the absorption edge. Different choices of the weight, which can depend on the system under study, are possible, and a systematic analysis of this problem will be the object of a forthcoming paper.

3. Theory *vs* theory

To test that the computational procedure works correctly and it is able to probe structural parameters, we have performed a theoretical test on the Ni *K*-edge of the octahedrally coordinated NiO_6. The XANES spectrum of NiO_6 has a well defined shape with a very big resonance at the edge formed by the coherent sum of MS contributions all in phase at the resonance energy (Benfatto *et al.*,

1986). This structure is really a full MS resonance, as it cannot be correctly reproduced by a finite expansion of the MS series. At higher energy, beyond about 50 eV, where the MS series expansion converges, a destructive interference occurs between pairs of consecutive MS terms, making the EXAFS signal the only relevant contribution, although higher-order terms are quite sizable and comparable in magnitude with the EXAFS signal up to 150 eV. This seems a general effect in octahedral clusters of transition metals. Actually, the best quantitative agreement between experimental data and *ab initio* theoretical calculations, valid in the whole energy range, has been obtained for these systems using the complex HL potential. Some discrepancies are present in the first 20 eV from the edge due essentially to the overestimation of the inelastic losses (Benfatto *et al.*, 1997).

A pictorial view of this system is reported in Fig. 2. The origin of the coordinates is on the Ni atom. The polar coordinates of the oxygen ligands are the parameters to be optimised by *MXAN*. This test follows the coming strategy:

(i) The XANES spectrum of the NiO_6 octahedral cluster with a metal–oxygen distance of 2.0 Å is calculated by using the real part of the HL potential. Then a Gaussian noise is added to the calculation to mimic real experimental data. The intensity of this noise corresponds to a noise-to-signal ratio of about 1%, which is a typical value for experimental data for very diluted system, or time-resolved experiment. The spectrum is reported as dotted lines in Figs. 3, 4 and 5. It represents the experimental data to be fitted and corresponds to the known structure (K.S.), reported in Table 1.

(ii) Three different distortions to the oxygen coordination shell have been applied, representing the putative starting structures for the various *MXAN* minimization processes described later. More precisely: (*a*) as a first case (ST.1) all the distances $\mathbf{R}_{x1}$, $\mathbf{R}_{x2}$, $\mathbf{R}_{y1}$, $\mathbf{R}_{y2}$, $\mathbf{R}_{z1}$ and $\mathbf{R}_{z2}$ have been increased to 2.15 Å; this distortion determines an enormous value of the square residue in the fit with the K.S. structure; here $S^2/n = 106$; (*b*) as second case the starting structure (ST.2) has $\mathbf{R}_{x1} = \mathbf{R}_{x2} = 2.15$ Å, $\mathbf{R}_{y1} = \mathbf{R}_{y2} = 2.10$ Å, and $\mathbf{R}_{z1} = \mathbf{R}_{z2} = 1.85$ Å; here $S^2/n = 92$.
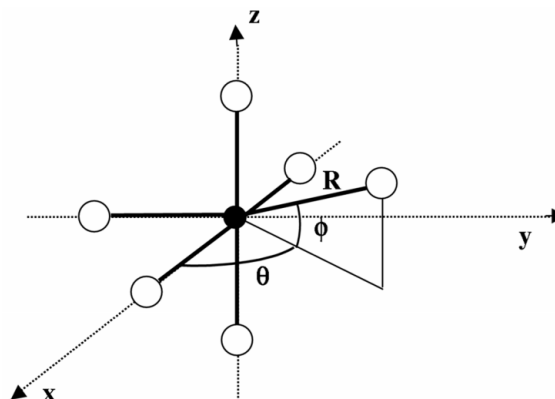

Figure 2
Pictorial view of the NiO_6 atomic cluster used in the present calculation. The central Ni atom is the black-filled circle. The polar coordinates **R**, θ and ϕ of the oxygen atoms are the parameters to be optimized by *MXAN*.

Table 1
Structural data related to the theory-*vs*-theory analysis described in the text.
The K.S. structure is an NiO_6 octahedron. $\Delta\theta$ represents an angular deviation from octahedral symmetry. $c(\mathbf{R_{x1}})$ refers to distances correlated to R_{x1}.

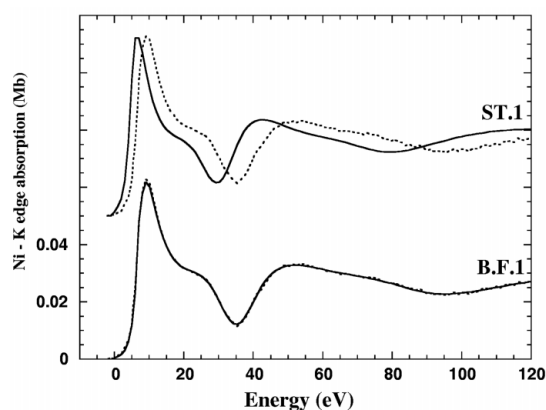|	S^2/n	$\mathbf{R_{x1}}$ (Å)	$\Delta\mathbf{\theta_{x1}}$ (°)	$\mathbf{R_{x2}}$ (Å)	$\Delta\mathbf{\theta_{x2}}$ (°)	$\mathbf{R_{y1}}$ (Å)	$\mathbf{R_{y2}}$ (Å)	$\mathbf{R_{z1}}$ (Å)	$\mathbf{R_{z2}}$ (Å)
K.S.	-	2.00	0.0	2.00	0.0	2.00	2.00	2.00	2.00
ST.1	106.0	2.15	-	2.15	-	2.15	2.15	2.15	2.15
B.F.1	1.3	2.00	-	$c(\mathbf{R_{x1}})$	-	$c(\mathbf{R_{x1}})$	$c(\mathbf{R_{x1}})$	$c(\mathbf{R_{x1}})$	$c(\mathbf{R_{x1}})$
ST.2	92.0	2.15	-	2.15	-	2.10	2.10	1.85	1.85
B.F.2	1.3	1.99	-	2.00	-	2.01	2.00	2.02	2.03
B.F.3	10.6	1.99	-	1.99	-	1.99	1.99	2.01	2.01
B.F.4	5.7	2.00	-	1.96	-	1.98	1.99	2.00	2.05
ST.3	62.0	2.15	+10.0	2.15	-10.0	-	-	1.85	1.85
B.F.5	1.3	2.01	+1.8	2.02	-1.2	-	-	1.99	2.01

Figure 3
Theory-*vs*-theory best-fit results obtained starting from structure ST.1 in a single parameter space. All the θ and ϕ polar coordinates of the oxygens are kept fixed, while the R coordinates are fully correlated. The uppermost curves represent the comparison between the K.S. (dotted line) and the ST.1 (solid line) calculations. The lowermost curves represent the K.S. (dotted line) and the best-fit result B.F.1 (solid line).
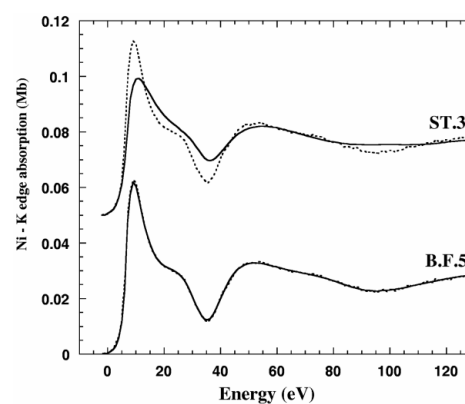

Figure 4
Theory-*vs*-theory best-fit results obtained starting from structure ST.2 (solid line) in a six parameters space. All the θ and ϕ polar coordinates of the oxygen atoms are kept fixed, while the R coordinates are independent. Dotted lines: K.S. structure. The numerical results of B.F.2 (no statistical weight, potential recalculated), B.F.3 (no statistical weight, potential kept fixed) and B.F.4 (with statistical weight, potential kept fixed) are described in Table 1.

Figure 5
Theory-*vs*-theory best fit result B.F.5 obtained starting from structure ST.3 in the space of two θ polar angles and four distances. Dotted lines: K.S. structure. The numerical results are described in Table 1.

In the last case, in the starting structure (ST.3), $\mathbf{R_{y1}}$ and $\mathbf{R_{y2}}$ are left undistorted, $\mathbf{R_{x1}} = \mathbf{R_{x2}} = 2.15$ Å, and $\mathbf{R_{z1}} = \mathbf{R_{z2}} = 1.85$ Å; moreover, the angular parameters θ_{x1} and θ_{x2} are changed, respectively, by +10° and −10°. This distortion gives $S^2/n = 62$.

(iii) By using the *MXAN* procedure we recover the known structure K.S. from the different starting conditions, with an accuracy that depends on the options used for the potential and for the weighting function. The results are summarized in Table 1.

The first best-fit procedure, B.F.1, starts from structure ST.1 and optimises the S^2 value in the parameters space of a single distance, *i.e.* all the Ni–O distances are considered as a single parameter and change simultaneously. No statistical weight is used, and the potential is recalculated at each step. The B.F.1 procedure recovers the correct structure K.S. with a value $S^2/n = 1.3$ reaching a statistical error of 0.007 Å in the distance determination, as evaluated by the *MIGRAD* algorithm of the *MINUIT* package. This value can be considered the best theoretical limit for the structural resolution of a single independent distance parameter in the octahedral systems, for the chosen noise-to-signal ratio. The comparison between the K.S., ST.1 and B.F.1 spectra is reported in Fig. 3.

A second group of calculations are shown in Fig. 4. They are performed starting from the putative structure ST.2 that represents a highly distorted octahedron with a spread of the Ni–O distance of ±0.15 Å.

The B.F.2 procedure optimises the S^2 value in a six parameters space, *i.e.* the six Ni–O distances move independently. No statistical weight is used, and the MT potential is recalculated at each step, as
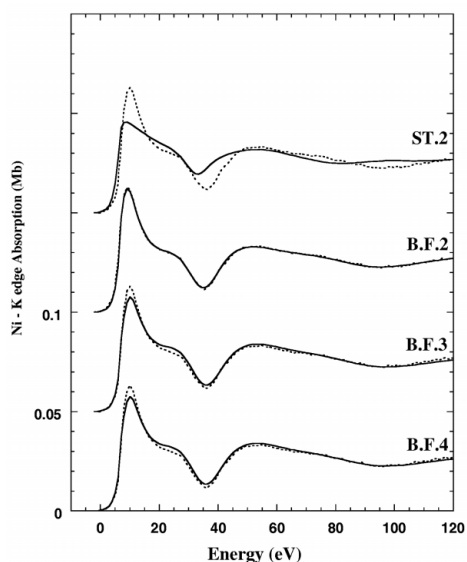
in the case of B.F.1 procedure. The correlation matrix between the six parameters was calculated and its effect on the statistical error of the fitted distances was evaluated. The K.S. structure is recovered as in the previous case, leading to the same value of $S^2/n = 1.3$, but with a spread of the metal–oxygen distances of about ±0.03 Å. This value, higher than the previous one, is due to the correlation between the different parameters. It can be assumed as the best theoretical limit for structural resolution of metal–ion distances.

The strategy B.F.3 is performed by keeping the potential fixed to that of structure ST.2, in particular the muffin tin radii are calculated on the basis of the starting geometrical structure. No statistical weight is used. At the best-fit conditions, S^2/n increases enormously, going to 10.6, and small discrepancies appear in the intensity of the various features at about 20 eV between the fitted spectrum and the 'experimental' data of the K.S. structure. These effects are due to the potential errors induced essentially by the wrong choice of the MT radii, calculated on the basis of the putative structure. Nevertheless the best-fitting structure B.F.3 is fully consistent with the K.S. structure (see Table 1 and Fig. 4) confirming that the atomic arrangement around the absorber dominates the shape of the XAS spectrum.

The best-fit B.F.4 is performed under the same conditions as B.F.3, apart from using a statistical weight as defined in the second paragraph. Here we are assuming that the potential has low reliability and it can introduce artefacts at energies below 30 eV. The best-fitting S^2/n decreases to 5.7. The best-fitting structure B.F.4 is still fully consistent with the K.S. structure (see Table 1) although the spread of the metal–oxygen distances is now increased to ±0.05 Å.

The last best-fit strategy B.F.5 starts from the putative structure ST.3, which is obtained from the regular octahedron by moving angles and distances. The optimization of the S^2 function is achieved in the parameter space formed by four Ni–O distances and two angles, without the use of any weight w_i. The potential is recalculated at each step. In this case the best-fit condition is reached for $S^2/n = 1.3$, that is a value equal to the B.F.1 and B.F.2 strategies, and the best-fitting structure is fully consistent with the K.S. geometry (Table 1) within a spread of the metal–oxygen distances of about ±0.03 Å and of the θ angles of about ±2.0°. The comparison between the K.S., ST.3 and B.F.5 spectra is reported in Fig. 5.

It seems necessary to make here a brief comment on the problem of the number n of independent parameters in the data analysis in the XANES range. The problem is a very complicated mathematical task, due to the non-linear dependence of the signal from the structural parameters. Nevertheless, the number of independent parameters can be numerically estimated case by case, by looking at both the correlation matrix and the contour plots (Filipponi, 1995; Michalowicz & Vlaic, 1998), related to the parameters of the subspace chosen for the fitting, *via* the subroutines in the *MINUIT* program. This analysis can be easily performed with our method, because the number of structural parameters is small; we do not have to fit Debye–Waller factors and coordination numbers. We note that Stern's criterion $n < 2 + 2\Delta k \Delta r/\pi$ (Stern, 1993) applied to our case gives $n < 9$ where $\Delta k \cong 6$ Å^{-1} and $\Delta r = 2$ Å. In the previous analysis the B.F.2 strategy is the only case affected by an appreciable correlation between the six parameters; for brevity, the related correlation matrix and the contour plots are not reported.

These theoretical tests show the ability of the *MXAN* procedure to recover the correct geometrical environment around an absorber independently from the starting putative structure. The precision of distance determination is comparable with that obtained in the

EXAFS spectroscopy and the sensitivity to the angles is enough to be hopefully used for practical applications. It is noticeable that these results are obtained with an experimental noise-to-signal ratio for which it will be very difficult to perform EXAFS analysis.

A similar study has been applied to the XAS spectrum of Zn in the distorted tetrahedral site of the protein superoxide dismutase (Benfatto *et al.*, 2001) obtaining a precision in the structural determination comparable with the present case. These examples support the idea of a one-to-one correspondence between the geometrical structure and shape of the XANES spectrum and the possibility of using the XANES spectroscopy for quantitative structural determination.

4. Theory-*vs*-experiment

In this section we show the ability of the *MXAN* procedure to recover the correct geometrical structure using experimental XANES data of Ni^{2+} in aqueous solution. The data at the Ni *K*-edge have been recorded in transmission mode using a Mylar cell at beam station 7.1 of Daresbury Laboratory. A double-crystal Si(111) monochromator was used and the storage ring was operated at 2 GeV with an average current of 150 mA. The sample was prepared by dissolving $NiCl_2$ in water to obtain a solution of 5 mM. The pH was controlled in order to have the hydrated species Ni^{2+} ion. The background contribution from previous edges was fitted with a linear function and subtracted from the raw data.

Starting from a distorted geometrical structure, we have used different fitting strategies to recover the correct octahedral configuration, by changing the parameters in the subspace formed by the metal–oxygen bond lengths. No hydrogen atoms have been included in the calculation of the spectra, since they have a role only in the rising edge of the spectrum (Benfatto *et al.*, 1997).

First, we present the results obtained by using the complex HL potential for the exchange-correlation part. In this case, the complex part of the HL potential introduces an over damping of the calculated spectra in the low-energy part of the XAS spectrum (Benfatto *et al.*, 1997; Rehr & Albers, 2000). This circumstance implies a theoretical calculation smoother than the experimental data in this energy region with some spectral features hidden by the inelastic losses. Therefore, the statistical weight w_i of section 2, with the same parameters E_c and Θ, has been used. The potential has been recalculated at every step during the procedure.

In Fig. 6 we report the comparison between the experiment (dotted lines) and the calculations for the starting geometrical configuration St and the two different final structures obtained by the fitting procedure using a different number of parameters. Here the starting structure St is an octahedron formed by six oxygen atoms at a distance of 2.15 Å from the metal ion. The mismatch between the experimental data and the St calculation reflects the wrong oxygen–metal distance. Curve p.1 corresponds to the best-fit condition reached by moving just one parameter, *i.e.* all the six oxygen–metal bonds have the same distance value and are forced to move simultaneously during the minimization procedure. The minimum corresponds to an octahedron with an oxygen–metal distance of 1.99 Å to be compared with a known distance of 2.02 ± 0.03 Å. The lowermost solid curve, indicated as p.5, corresponds to the best-fit condition reached by moving five parameters, *i.e.* four bond lengths are left independent and the last two are linked. The minimum corresponds to an octahedron with an oxygen–metal

Table 2
Structural data related to the theory-vs.-experiment analysis described in the text.

The St. structure is a starting putative structure of the Ni^{2+} in water solution. $c(R_{x1})$ refers to distances correlated to R_{x1}. Numbers in parentheses represent the statistical error on the last digit as evaluated by the routine *MIGRAD* of *MINUIT*.

	S^2n	R_{x1} (Å)	R_{x2} (Å)	R_{y1} (Å)	R_{y2} (Å)	R_{z1} (Å)	R_{z2} (Å)
St.	17.8	2.15	2.15	2.15	2.15	2.15	2.15
p.1	5.4	1.99(1)	$c(R_{x1})$	$c(R_{x1})$	$c(R_{x1})$	$c(R_{x1})$	$c(R_{x1})$
p.5	5.4	1.99(1)	$c(R_{x1})$	1.99(1)	1.99(1)	1.99(1)	1.99(2)

Table 3
Structural data related to the theory-vs.-experiment analysis described in the text.

The St.1 structure is a different starting putative structure of the Ni^{2+} in water solution. $c(R_{x1})$ refers to distances correlated to R_{x1}. Numbers in parentheses represent the statistical error on the last digit as evaluated by the routine *MIGRAD* of *MINUIT*.

	S^2/n	R_{x1} (Å)	R_{x2} (Å)	R_{y1} (Å)	R_{y2} (Å)	R_{z1} (Å)	R_{z2} (Å)
St. 1	12.0	2.07	2.07	2.10	2.10	1.92	1.92
p. 3	5.4	1.99(1)	$c(R_{x1})$	1.99(1)	$c(R_{y1})$	1.99(2)	$c(R_{z1})$
p. 6	5.4	1.99(2)	1.99(1)	1.99(1)	1.98(1)	1.99(1)	1.99(2)

distance of 1.99 Å. Table 2 summarizes these results with the value of the S^2/n function and the statistical errors evaluated by the routine *MIGRAD* of *MINUIT*.

As expected, the agreement between the experimental data and the fitting calculations are good in the energy range from 35 eV to 140 eV, while relevant discrepancies are present at lower energy, between 10 eV and 35 eV, due the overestimation of the inelastic losses of the HL potential. In particular the spectral feature at about 30 eV is completely absent. The best agreement between the calculation and the experiment results in a value of S^2/n about five times higher than in the ideal case of the theory-*vs*-theory comparison. Nevertheless, the results confirm the possibility to recover the correct geometrical environment around the absorbing site in spite of the presence of several approximations in the numerical determination of potential.

In Fig. 7 we report a second set of results obtained by starting from a putative geometrical configuration St.1, with orthorhombic symmetry, where the pairs of opposite oxygen atoms have a distance from the central nickel ion of 1.92 Å, 2.07 Å and 2.10 Å, respectively. Curve p.3 corresponds to the best-fit condition obtained by moving three parameters, *i.e.* the opposite atoms in each pair are forced to move jointly during the procedure. The best-fit corresponds
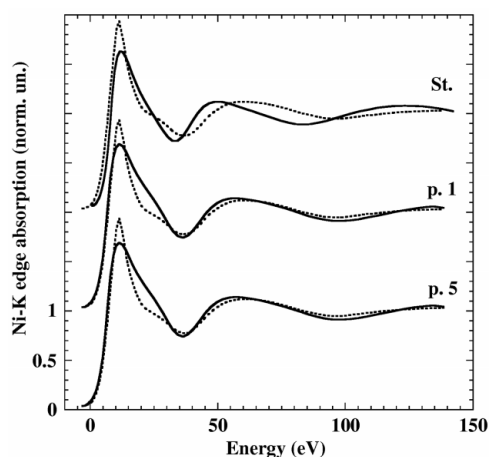

Figure 6
Theory-*vs*-experiment best-fit results obtained starting from structure St. The experimental data are depicted by dotted lines. The uppermost curves show the comparison between the experimental data and the calculation related to structure St. (solid line). p.1 : best fit in a single parameter space (all the distances are correlated). p.5: best fit in a five parameters space. The numerical results are described in Table 2.
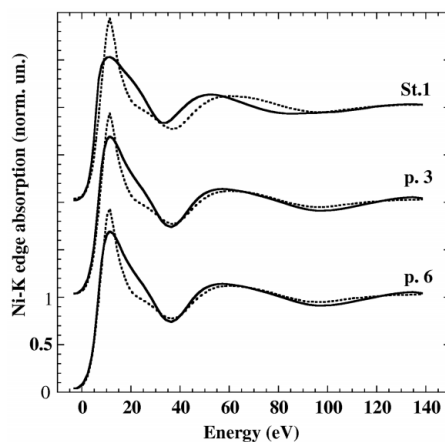

Figure 7
Theory-*vs*-experiment best-fit results obtained starting from structure St.1. The experimental data are depicted by dotted lines. The uppermost curves show the comparison between the experimental data and the calculation related to structure St.1 (solid line). p.3 : best fit in a three parameters space (all the distances are correlated). p.6: best fit in a six parameters space. The numerical results are described in Table 3.

to an octahedral symmetry with an oxygen–metal distance of 1.99 Å as found in the previous set of fitting calculations. The quality of the fit is equal to the previous cases, as shown by the value of the S^2/n function reported in Table 3. The last curve p.6 shows the case of a fit with six parameters: each bond length is left independent. The best-fit condition still corresponds to octahedral symmetry with all the oxygen–metal distances equal to 1.99 Å with $S^2/n = 5.4$. The summary of this second set of fitting results is reported in Table 3.

These calculations show the ability of the *MXAN* procedure to recover the correct geometrical configuration in a real case independently from the starting putative structure and the number of parameters. The minimum of the fit corresponds to a unique geometrical solution with a well-defined symmetry and Ni–O distances. It is noticeable that this result has been obtained despite the presence of relevant discrepancies between the theoretical calculations and the experimental data in the very low energy part of the spectrum, mainly due to errors in the determination of the potential. A judicious choice of the weight w_i minimises the effects of these errors on the structural refinement. Our results clearly show the high sensitivity of the XANES spectroscopy to the geometrical arrangement of the atoms rather than to the details of the potential.

At the same time, these results demonstrate that the use of the HL potential is not completely adequate in the case of molecular systems. Clearly, the discrepancies between fits and experimental data in the low-energy part of the spectrum make the use of this region difficult to extract any type of information. For this reason we have repeated the fitting procedure by accounting for all the inelastic processes *via* the convolution of the total cross section, calculated using the real part of the HL potential, with a broadening Lorentzian function, as described in section 2. The total width is defined as $\Gamma = \Gamma_c + \Gamma(E)$ where Γ_c includes the core-hole lifetime plus the experimental resolution and $\Gamma(E)$ represents all the inelastic processes suffered by the photoelectron during the scattering events in the system. Both terms are adjusted during the fit procedure.
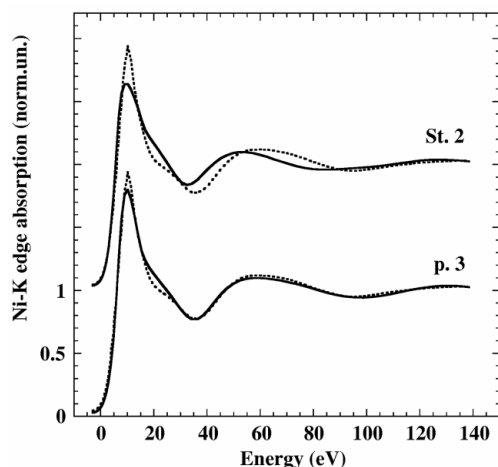

Figure 8
Theory-*vs*-experiment best-fit results obtained starting from structure St.2 The experimental data are depicted by dotted lines. Here the calculations are made by accounting for all the inelastic processes *via* a convolution of the total cross section, with Lorentzian function. The uppermost curves show the comparison between the experimental data and the calculation related to structure St.2. p.3: best fit in a three parameters space. The numerical results are described in the text.

In Fig. 8 we report the results obtained with this strategy. The uppermost curves show the comparison between the experimental data and the calculation related to the starting geometrical configuration St.2, formed by a cluster with orthorhombic symmetry and an Ni–O distance of the pairs of opposite oxygen atoms of 1.90 Å, 2.10 Å and 2.15 Å, respectively. Curve p.3 corresponds to the best-fit condition obtained by changing three parameters, *i.e.* the *MXAN* procedure moves the Ni–O distances and the opposite atoms in the cluster are forced to move simultaneously during the minimisation. Γ_c and $\Gamma(E)$ are refined by the program. The experimental data are reported as dotted lines in the figure.

The best fit corresponds to an octahedral symmetry with an oxygen–metal distance of 2.00 ± 0.04 Å. A value of $\Gamma_c = 2.6 \pm 0.25$ eV results from the procedure while the energy-dependent part has an onset at 14.5 ± 1.6 eV and amplitude of 6.1 ± 2.0 eV. The constant part Γ_c is in good agreement with the sum of the core-hole lifetime (~1 eV) plus the experimental resolution that is about 1.3 eV in our experimental condition. No weight w_i has been used in this case. The S^2/n function decreases to about 2.3, a value just two times higher than in the ideal case of the theory-*vs*-theory comparison. The agreement between the experimental data and theoretical curve is now good in the whole energy range, the very small discrepancies at low energy being essentially due to the absence of the hydrogen atoms in the calculation.

5. Conclusions

The new package *MXAN* presented here allows a quantitative analysis of the XANES spectrum in the whole energy range, *i.e.* from the edge to about 200 eV. For the first time this spectroscopy has been used to derive quantitative geometrical information with a full statistical determination of the uncertainty of the parameters. It has been possible to evaluate the best theoretical limit for the structural resolution (distances and angles) in the case of the NiO_6 cluster by the theory-*vs*-theory comparison, and the application to different system confirms the possibility for the XANES spectroscopy to give structural information at atomic resolution (Benfatto *et al.*, 2001).

The application to real experimental data has allowed one to recover the correct octahedral configuration of the Ni^{2+} ion in aqueous solution with an accuracy comparable with EXAFS spectroscopy (± 0.04 Å). The minimum of the fit has been reached independently of the starting configuration and the number of the parameters, confirming the intuitive assumption of a one-to-one relationship between the XANES spectra and the structural configurations. It is noticeable that the correct geometrical structure of the Ni^{2+} ion can been obtained independently from approximations in the numerical determination of potential, through a judicious choice of the statistical weight function. The use of a phenomenological broadening function to mimic the inelastic losses improves considerably the quality of the fit making the very low energy region accessible for quantitative analysis. This fact is particularly important for applications such as diluted and/or disordered systems like proteins, time-resolved studies, and in general studies for which the signal decreases so rapidly with the energy to make the standard EXAFS analysis difficult to be performed.

Helpful to theorists would be the modularity of the *MXAN* procedure. New kinds of potentials, especially in the exchange-correlation part, could be easily introduced at each step of the calculation, opening the possibility for numerical comparison

between different types of approximation. Applications to systems with a high degree of structural disorder are possible as well by *ab initio* calculations using the augmented space formalism (Benfatto, 1995), allowing the study of alloys or multiple site systems.

References

Benfatto, M. (1995). *Physica B*, **208/209**, 42–44.

Benfatto, M., Natoli, C. R., Bianconi, A., Garcia, J., Marcelli, A., Fanfoni, M. & Davoli, I. (1986). *Phys. Rev B*, **34**, 5774–5781.

Benfatto, M., Solera, J. A., Chaboy, J., Proietti, M. G. & Garcia, J. (1997). *Phys. Rev B*, **56**, 2447–2452.

Benfatto, M., Congiu-Castellano, A., Daniele, A. & Della Longa, S. (2001). *J. Synchrotron Rad.* **8**, 267–269.

Binsted, N. & Hasnain, S. S. (1996). *J. Synchrotron Rad.* **3**, 185–196.

Briois, V., Lagarde, P., Brouder, C., Sainctavit, Ph. & Verdaguer, M. (1995). *Physica B*, **208**/**209**, 51–52.

Cabaret, D., Joly, Y., Renevier, H. & Natoli, C. R. (1999). *J. Synchrotron Rad.* **6**, 258–260.

Chou, S. H., Rehr, J. J., Stern, E. A. & Davidson, E. R. (1987). *Phys. Rev. B*, **35**, 2604–2614.

Cruickshank, D. W. J. (1999). *Acta Cryst.* D**55**, 583–601.

Della Longa, S., Soldatov, A., Pompa, M. & Bianconi, A. (1995). *Comput. Mat. Sci.* **4**, 199–210.

Della Longa, S., Pin, S., Cortes, R., Soldatov, A. & Alpert, B. (1998). *Biophys. J.* **75**, 3154–3162.

Durham, P., Pendry, J. B. & Hodges, C. H. (1982). *Comput. Phys. Commun.* **25**, 193–200.

Enderby, J. E. & Neilson, G. W. (1981). *Rep. Prog. Phys.* **44**, 593–613.

Filipponi, A. (1995). *J. Phys. Condens. Matter,* **7**, 9343–9356

Filipponi, A. & Di Cicco, A. (1995). *Phys. Rev. B*, **52**, 15135–15144.

Foulis, D. L., Pettifer, R. F. & Sherwood, P. (1995). *Europhys. Lett.* **29**, 647–652.

Garcia, J., Bianconi, A., Benfatto, M. & Natoli, C. R. (1986). *J. Phys. (France) Colloq.* **47**, C8:49–54.

Hasnain, S. S. & Hodgson, K. O. (1999). *J. Synchrotron Rad.* **6**, 852–864.

Hedin, L. & Lundqvist, S. (1969). *Solid State Phys.* **23**, 1–15.

James, F. (1994). Cern Program Library Long Writeup D506. (Also available at http://wwwinfo.cern.ch.asdoc.minuit.)

Lagarde, P., Fontaine, A., Raoux, D., Sadoc, A. & Migliardo, P. (1980). *J. Chem. Phys.* **72**, 306–314.

Michalowicz, A. (1997). *J. Phys. IV Coll. C*2, pp. 235–236, and references therein.

Michalowicz, A. & Vlaic, G. (1998). *J. Synchrotron Rad.* **6**, 1317–1320.

Muller, J. E., Jepsen, O. & Wilkins, J. W. (1982). *Solid State Commun.* **42**, 365–368.

Natoli, C. R. & Benfatto, M. (1986). *J. Phys. (France) Colloq.* **47**, C8:11–23.

Natoli, C. R., Benfatto, M. & Doniach, S. (1986). *Phys. Rev. A*, **34**, 4682–4694.

Natoli, C. R., Benfatto, M., Brouder, C., Ruiz Lopez, M. F. & Foulis, D. L. (1990). *Phys. Rev. B*, **42**, 1944–1968.

Norman, J. G. (1976). *Mol. Phys.* **31**, 1191–1198.

Rehr, J. J. & Albers, R. C. (2000). *Rev. Mod, Phys.* **72**, 621–654.

Stern, E. A. (1993). *Phys. Rev. B*, **48**, 9825–9827.

Tyson, T. A., Hodgson, K. O., Natoli, C. R. & Benfatto, M. (1992). *Phys. Rev. B*, **46**, 5997–6019, and references therein.